PCCP

Molecular Dynamics Study of The Effect of Alkyl Chain Length on Melting Points of $[C_nMIM][PF_6]$ Ionic Liquids

Yong Zhang and Edward J. Maginn[*]

Department of Chemical and Biomolecular Engineering

University of Notre Dame

Notre Dame, Indiana, 46556

April 24, 2014

[*]Corresponding author. E-mail: ed@nd.edu

1

Abstract

Based on molecular dynamics simulations, the melting points T_m of a series of 1-alkyl-3-methylimidazolium hexafluorophosphate ionic liquids $[C_n MIM][PF_6]$ with n = 2, 4, 10, 12, and 14 were studied using the free energy-based pseudosupercritical path (PSCP) method. The experimental trend that the T_m decreases with increasing alkyl chain length for ILs with short alkyl chains and increases for the ones with long alkyl chains was correctly captured. Further analysis revealed that the different trends are the results of the balance between fusion enthalpy and fusion entropy. For the ILs with short alkyl chains (ethyl and butyl groups), fusion entropy plays the dominant role so that $[C_4 MIM][PF_6]$, which has a larger fusion entropy due to its higher liquid phase entropy has the lower melting temperature. As for the ILs with long alkyl chains, due to the enhanced van der Waals interactions brought about by the long non-polar alkyl chains, enthalpy becomes the deciding factor and the melting points increase when the alkyl chain goes from C10 to C14. While the melting points for $[C_2 MIM][PF_6]$ and $[C_4 MIM][PF_6]$ were quantitatively predicted and the trends for the long chain ILs were captured correctly, the absolute melting points for $[C_{10} MIM][PF_6]$, $[C_{12} MIM][PF_6]$ and $[C_{14} MIM][PF_6]$ were systematically overestimated in the simulations. Three possible reasons for the overestimation were studied but all ruled out. Further simulation or experimental studies are needed to explain the difference.

1   Introduction

Ionic liquids (ILs) are a group of salts with relatively low melting points T_m (usually lower than 100 °C). During the past decade, various experimental and theoretical techniques have been applied to study ionic liquids.[1–9] Besides their unique properties such as low T_m, negligible vapor pressure, non-flammability, and good ionic conductivity, the other reason why ionic liquids have drawn extensive attention over the past years is because of the possibility to fine-tune their properties for various applications. It is for this reason that ionic liquids are sometimes called designer solvents.

By combining different cations and anions, there are potentially a large number of compounds that can be ionic liquids. The properties of these ionic liquids can be totally different and suit different applications. Even for ionic liquids with similar cations and anions, the properties can be quite different. The most widely studied imidazolium-based ionic liquids serve as one such example. In this group of ILs, when the hydrogen atom at the C2 position of the imidazolium ring is replaced by a methyl group, the liquid structure, dynamic and thermodynamic properties change dramatically due to the change in the intermolecular interaction and the subsequent changes in the configurational space.[10–16]

For the same imidazolium-based ILs, properties can also be tuned by changing the alkyl chain length attached to the imidazolium ring.[17–27] The liquid phase structure of these systems has been the focus of many studies. With short chains (n=1 or 2), the liquid phase is essentially homogeneous. When the alkyl chain becomes longer, the chains tends to self-aggregate due to hydrophobic interactions and form heterogeneous domains. Such behavior was first observed in molecular simulations[28–30] and confirmed later by small angle X-ray scattering experiments.[31] These systems were further studied subsequently by various computational and experimental techniques.[32–36] However, the exact structure of these liquids is still under debate.[37–39] Associated with the liquid phase structure, the dynamic properties change as well. For example, multiple experimental results have shown that the viscosity of the ionic liquids increases when the length of the alkyl chain increases.[10, 18, 40–42] Similar behavior was also observed for the enthalpy of vaporization.[43–47] Enhanced van der Waals (vdW) interactions were suggested to play an important role in these effects.[10, 43, 44]

On the other hand, the melting points, one of the key features of ionic liquids as indicated by their definition, show more complicated behavior. For ILs formed by 1-alkyl-3-methylimidazolium ($[C_nMIM]$) and hexafluorophosphate ($[PF_6]$) or tetrafluoroborate ($[BF_4]$), a non-monotonic behavior was observed for T_m as a function of chain length.[48] For $[C_nMIM][PF_6]$ with short alkyl chains, T_m decreases when the chain length increases until a minimum is reached for $[C_6MIM][PF_6]$ and $[C_8MIM][PF_6]$. After that, when the alkyl chain becomes longer, T_m increases. Similar behavior was observed for $[C_nMIM][BF_4]$ ILs except that the minimum T_m was observed for ILs with chains having five to nine carbons.[48] In spite of these rather remarkable observations, relatively little fundamental work has been done to understand and predict melting point trends in ILs. QSPR or group contribution methods have been developed to correlate the molecular structure and T_m of ionic liquids. Great success has been seen in the literature but due to the lack of physical insight, the accuracy of such methods are usually limited to ionic liquids having structures similar to those used in the training set. For complicated melting point behavior such as the alkyl chain length dependence mentioned above, such methods can not even predict the trend.[49,50] Actually, accurate calculation of T_m of compounds such as ionic liquids has been a challenge for computational chemistry, and we have shown that rigorous free energy based method are required.[51] Recently, using the pseudosupercritical path (PSCP) method, we studied $[C_4MIM][PF_6]$ and $[C_2MIM][PF_6]$ from the $[C_nMIM][PF_6]$ series and their C2 methylated counterparts $[C_4MMIM][PF_6]$ and $[C_2MMIM][PF_6]$.[16] The T_m of each IL was calculated and the trend that the C2 methylated ILs have higher T_m than the C2 protonated ILs was successfully captured. It was found that the origin of the higher T_m for the former is mainly entropic. In the present work, we extend the previous work to three $[C_nMIM][PF_6]$ ILs with longer alkyl chains, with n=10, 12, and 14, respectively, and focus on the effect of alkyl chain length on the melting points. The simulation details are described in the next section. The simulation results are presented and discussed after that. A summary is provided in the last section.

2 Methodology and Simulation Details

The T_m was calculated for each ionic liquid using the free energy-based pseudosupercritical path (PSCP) method.[51,52] Simulation details closely followed that described in our previous publication.[16] Briefly, classical molecular dynamics (MD) simulations were carried out using the LAMMPS package.[53] The general Amber force field (GAFF)[54] was used to describe the inter- and intramolecular interactions. Parameters for the P-F bond in the anion are not available in GAFF and were taken from the literature.[55] The atomic charges were derived using the ESP method[56] by fitting the electrostatic potential surface generated from ab initio molecular dynamics (AIMD) simulations carried out on the crystal phase of each IL, as detailed in our previous publication.[52] A crystal unit cell[11,57,58] containing four ion pairs (200, 224 and 248 atoms for $[C_nMIM][PF_6]$ with n = 10, 12 and 14, respectively) were used for each IL. AIMD simulations were carried out using the CPMD package[59] with periodic boundary conditions. As shown previously,[52] the charge transfer and the effect of polarizability in bulk ionic liquid systems are implicitly considered in this method. This method has been found to be efficient and reliable.[16,52]

The crystal phase of the simulation systems were built up by reproducing the corresponding crystal unit cell[11,57,58] in the X, Y and Z directions. A total of 400 ion pairs for $[C_2MIM][PF_6]$, 250 pairs for $[C_4MIM][PF_6]$, and 192 pairs for $[C_nMIM][PF_6]$ (n = 10, 12, 14) were included in the simulation box, respectively. The initial liquid phase systems were prepared by putting the same number of ionic liquid molecules randomly in a cubic box. For both crystal phase and liquid phase simulations, the initial boxes were equilibrated for a time period of 2 ns in the isothermal-isobaric (NPT) ensemble, which was found to be long enough for all the systems under study. Canonical (NVT) ensemble simulations were then carried out under the equilibrium density. The pressure was fixed to be one atmosphere in all constant pressure simulations with isotropic volume fluctuations for the liquid phase and anisotropic cell for the crystalline phase. The temperature and pressure were controlled by the Nosé-Hoover thermostat[60] and the extended Lagrangian approach,[61] respectively.

3 Results and Discussions

3.1 Partial Charges

Using the AIMD-based method,[52] atomic partial charges were derived for each IL. The results are provided in the Electronic Supplementary Information. Total charges of ± 0.891 e, ± 0.902 e and ± 0.898 e were found for the cations and anions of $[C_{10}MIM][PF_6]$, $[C_{12}MIM][PF_6]$ and $[C_{14}MIM][PF_6]$, respectively (see Table 1). These values are larger (in absolute value) than those of $[C_2MIM][PF_6]$ and $[C_4MIM][PF_6]$, both of which were found to be about ± 0.8 e.[52] This difference is likely due to the reduction in charge transfer and polarization in the less polar environment of the ILs having long alkyl chains.

The atomic charges of the anion atoms as well as the heavy atoms in the imidazolium ring of the cations are shown in Figure 1 for each IL. The atomic labeling is shown in Figure 2. As the alkyl chain becomes longer from n=2 to n=14, the N3 atom shows the largest charge variation among the imidazolium ring atoms. For the anion, the magnitude of the charges on both P and F atoms increased with increasing cation chain length, although the total charges on the cations and anions did not change much. It is interesting to note that the atomic charge magnitude of the P and F atoms increase almost linearly as a function of alkyl chain length of the cation (see Figure 1).

3.2 Melting Points

Using the PSCP method,[51] the T_m were calculated to be 392 K, 411 K, and 438 K for $[C_{10}MIM][PF_6]$, $[C_{12}MIM][PF_6]$, and $[C_{14}MIM][PF_6]$, respectively. Their experimental T_m were measured to be 304 K, 333 K and 350 K, respectively.[11,58] A systematic overestimation of about 80-90 K was observed for the simulated results. This is different from the almost exact agreement with experimental results for the smaller ILs $[C_2MIM][PF_6]$ and $[C_4MIM][PF_6]$ in the series.[16] However, as shown in Figure 3, the trend in the experimental T_m that the elongation of the alkyl chain by two CH_2 group causes an increase of about 20 K in the T_m was correctly captured. The possible reasons that cause the overestimated T_m for the long alkyl chain ILs will be discussed later.

For each IL $[C_nMIM][PF_6]$ with n=2, 4, 10, 12 and 14, the fusion enthalpy (ΔH_f) and fusion entropy (ΔS_f) at the melting temperature were computed from the simulations. Near the melting temperature, the crystal phase starts to destabilize for the ILs having long chains, which introduces an error in the calculated enthalpy. To minimize the error, the enthalpies as a function of temperature were fit to a linear function in the low temperature range for all the ILs. To be consistent, the same procedure was also applied to the liquid phase. The fusion enthalpies were then calculated based on the linear fit and the results are summarized in Table 2. Available experimental results are also provided for comparison. Due to the small refinements in the calculation procedure used in the present study, the results for $[C_2MIM][PF_6]$ and $[C_4MIM][PF_6]$ in Table 2 are slightly different from those in Ref,[16] but the trend remains the same.

At the melting temperature, the free energies of the crystal and liquid phases are equal (i.e. $\Delta G_f = \Delta H_f - T\Delta S_f = 0$). A larger ΔH_f tends to lead to increased T_m, while a larger ΔS_f tends to lead to a decreased T_m. These two are in competition with one another and the balance between ΔH_f and ΔS_f decides the melting point. As shown in Table 2, both ΔH_f and ΔS_f are larger for $[C_4MIM][PF_6]$ than for $[C_2MIM][PF_6]$ by 0.63 kJ/mol and 10.71 J/mol/K, respectively. The fact that T_m is lower for $[C_4MIM][PF_6]$ than $[C_2MIM][PF_6]$ indicates that the entropic term controls the melting point trend for these two ILs. Similar behavior was observed in the experimental results, where ΔH_f of $[C_4MIM][PF_6]$ is about 2 kJ/mol larger than that of $[C_2MIM][PF_6]$ and ΔS_f of $[C_4MIM][PF_6]$ is 17.16 J/mol/K larger than that of $[C_2MIM][PF_6]$, although these values are slightly larger than the simulation results.

The accessible configurations in the liquid phase can behave as an indicator of the liquid phase entropy.[12, 13, 15, 23, 62] The anion center of mass distributions around cations were computed for $[C_2MIM][PF_6]$ and $[C_4MIM][PF_6]$ based on their liquid phase NVT ensemble trajectories. The results are shown in Figure 4. As shown in the figure, the spatial distribution function (SDF) for the anion around cation in both ILs share similar features. For instance, in both ILs, the H2 position in the cation imidazolium ring is the most favorable interaction site between cations and anions, consistent with previous studies.[14, 16] However, there are some differences. Relative to $[C_4MIM][PF_6]$, the anion has significantly less distri-

bution around the H5 position in $[C_2MIM][PF_6]$ although weaker repulsion is expected for the latter because of the smaller alkyl chain (ethyl group relative to butyl group). Such difference in the SDFs suggests fewer stable configurations in liquid $[C_2MIM][PF_6]$, indicating smaller entropy.[12]

For $[C_nMIM][PF_6]$ with long alkyl chains (n=10, 12 and 14), the calculated ΔH_f from the simulations are almost double the experimental results. The ΔS_f was also significantly overestimated from the simulation. However, like in the case of $[C_4MIM][PF_6]$ and $[C_2MIM][PF_6]$, both simulation and experimental results show the same trend. Based on the simulation results, when the alkyl chain is elongated by two carbons (from $[C_{10}MIM]$ to $[C_{12}MIM]$ or from $[C_{12}MIM]$ to $[C_{14}MIM]$), the ΔH_f increases by about 9.6 kJ/mol, which is about 15 times larger than the increase from $[C_2MIM][PF_6]$ to $[C_4MIM][PF_6]$. The increase in the calculated ΔS_f per two CH_2 groups in the alkyl chain was also found to be larger for the long chain ILs. The increase was found to be 18.71 J/mol/K from $[C_{10}MIM][PF_6]$ to $[C_{12}MIM][PF_6]$ and 14.64 J/mol/K from $[C_{12}MIM][PF_6]$ to $[C_{14}MIM][PF_6]$, about 75% and 37% larger than that from $[C_2MIM][PF_6]$ to $[C_4MIM][PF_6]$. In experiments, the difference in ΔH_f between $[C_{12}MIM][PF_6]$ and $[C_{14}MIM][PF_6]$ is 4.02 kJ/mol, two times larger than that between $[C_2MIM][PF_6]$ and $[C_4MIM][PF_6]$. Unlike the simulation results, the difference in experimental ΔS_f between $[C_{12}MIM][PF_6]$ and $[C_{14}MIM][PF_6]$ is less than half of that between $[C_2MIM][PF_6]$ and $[C_4MIM][PF_6]$. It is clear from both simulation and experimental results that for these long alkyl chain ILs, when the alkyl chain becomes longer, the increase in ΔH_f is more significant than the increase in ΔS_f. As a result, the enthalpic component of free energy plays the dominant role in deciding the melting points of ILs $[C_nMIM][PF_6]$ with n=10, 12 and 14, in contrast to the ILs with shorter chains where entropy dominates.

3.3 Cohesive Energy Analysis

In simulations based on classical force fields, the energy of the whole system is the sum of the bonded contributions such as bond, angle and dihedral angle energies, and non-bonded contributions including van der Waals (vdW) and electrostatic terms. The contribution of each energetic term to the calculated fusion enthalpy was analyzed and the results are

8

shown in Table 3. For comparison, the enthalpy of vaporization (ΔH_{vap}) of each IL was also calculated by following the procedure described previously[47] and the same energetic analysis was carried out. The results are summarized in Table 4. All the results shown in Tables 3 and 4 are at 298 K derived by extrapolating the energy $\sim$ temperature correlation based on linear fits.

At a given temperature, the kinetic energy contributes the same to enthalpy no matter what phase (solid, liquid or vapor) the system is in. As the result, for both solid-liquid transition and liquid-vapor transition, as shown in Tables 2, 3, and 4, the enthalpy differences can be well presented by the corresponding potential energy differences (ΔE_{pot}).

For enthalpy of vaporization, it is clear from Table 4 that, for each IL, the potential energy differences between the liquid and vapor phases are almost completely due to the differences in the nonbonded interactions (ΔE_{nb}) and the contribution from the bonded energies (ΔE_{bonded}) are negligible. The nonbonded energy can be further decomposed into electrostatic (ΔE_{elec}) and van der Waals (ΔE_{vdW}) terms. For $[C_4MIM][PF_6]$, the electrostatic contribution is slightly smaller than that of $[C_2MIM][PF_6]$. When the alkyl chain becomes longer, however, the electrostatic energy differences between vapor and liquid phases are about the same. The vdW contribution to the differences of ΔH_{vap} or ΔE_{pot}, on the other hand, keep increasing when the alkyl chains in the cations become longer. The increase per CH_2 group was found to be about 5 kJ/mol, which is consistent with the studies on other ILs or on homologous organic molecules.[47] It is interesting to notice that for the long alkyl chain ILs the increase in ΔE_{vdW} as a function of alkyl chain length matches that in ΔH_{vap} very well, which means that the increase in ΔH_{vap} for ILs with long alkyl chain in the cation is due to the enhanced van der Waals interactions of the hydrophobic chain, consistent with previous studies.[43,44]

As mentioned earlier, the fusion enthalpies of $[C_2MIM][PF_6]$ and $[C_4MIM][PF_6]$ are close to each other. As shown in Table 3, for these two ILs, the potential energy differences ΔE_{pot} between the solid and liquid phases are also close to each other. For the electrostatic component of the nonbonded energy, $[C_2MIM][PF_6]$ is larger than $[C_4MIM][PF_6]$ by 2.64 kJ/mol. In contrast, the vdW term is smaller for $[C_2MIM][PF_6]$ by about the same amount. These results are similar to the case of vaporization enthalpy.

For the ILs with a long alkyl chain in the cation, the fusion enthalpies (or potential energy differences between the two phases) keep increasing when the chain becomes longer, similar to that observed in liquid-vapor phase transition. However, as opposed to the vaporization enthalpies or fusion enthalpies of the small ILs, as shown in Table 3, ΔE_{bonded} contribution to ΔE_{pot} plays a more important role in these large ILs. These results suggests that, compared to the liquid-vapor phase transition or the solid-liquid phase transition of relatively small molecules, the melting process of the large ILs involves more significant intramolecular structural reorganization. On the other hand, even for these large ILs, ΔE_{pot} between solid and liquid phases is still dominated by the nonbonded interactions. For the two components of ΔE_{nb}, the increase in ΔE_{elec} per CH_2 group was found to be 0.8-0.9 kJ/mol and the increase in ΔE_{vdW} is more significant. Clearly, as with ΔH_{vap}, ΔE_{vdW} is still the most important contributor to ΔE_{pot} between solid and liquid phases or ΔH_f, and subsequently affects the melting points. But bonded energy as well as the electrostatic component of the nonbonded energy make significant contributions, too, which is different from the case of ΔH_{vap}.

3.4   Liquid Phase Structure and Dynamics

The role of vdW interactions in ionic liquids has been reported previously.[10,43,44] It was found that, when the alkyl chain becomes longer, the ILs tend to aggregate and the dynamics becomes slower.[10,18,28,29,31,40–42] For the reason of completeness, the liquid phase structure in terms of the center of mass (COM) radial distribution functions (RDFs) and site-specific RDFs and dynamic properties in terms of mean squared displacement (MSD) and self-diffusivity were calculated for each IL. The results are shown in Figures 5 and 6. In the calculation of center of mass, only the atoms in the imidazolium ring are considered for the cation. All atoms in the anion are included in the calculation of anion COM. The terminal carbon (CT) of the alkyl chain in the cations and the P atom in the anion were chosen for the site-specific RDFs.

In the COM RDFs, the height of the first peak increases when the alkyl chain becomes longer (the coordination number decreases, however, due to the decreases in number density in the bulkier ILs, results not shown), but the peak position and overall shape of the RDFs are similar in all ILs, indicating similar packing structure for the anion and the imidazolium

10

ring, which carries the most charges in the IL, in spite of the strong vdW interactions in the ILs with long alkyl chains. In the CT-P RDF, a structure is suggested by the peak at about 5 Å for $[C_2MIM][PF_6]$ and $[C_4MIM][PF_6]$. For the long alkyl chain ILs, this peak becomes less clear, indicating the loss of CT and P correlation. In CT-CT RDF, no clear structure can be observed in $[C_2MIM][PF_6]$, whereas a peak between 4 and 5 Å shows up in $[C_4MIM][PF_6]$. Then in $[C_nMIM][PF_6]$ with n=10, 12 and 14, two peaks, around 5 Å and 9 Å, respectively, are observed, which are the indicators of alkyl chain aggregation.[46] For the highly symmetric anion $[PF_6]$, as expected, the P-P site-site RDF is almost the same as anion-anion COM RDF.

Based on 20 ns NVT trajectories for $[C_2MIM][PF_6]$ and $[C_4MIM][PF_6]$ and 50 ns trajectories for other three ILs, the mean-square displacements (MSDs) of the ion center of mass were calculated and the self-diffusion coefficients were derived using the Einstein relation. The results are shown in Figure 6. Consistent with previous studies,[10, 18, 40–42] the dynamics in the liquid slow down significantly when the alkyl chain in the cation becomes longer. It is interesting to note that in the ILs with a short alkyl chain (ethyl or butyl), the cation diffuses faster than the anion, whereas in $[C_nMIM][PF_6]$ with n=10, 12 and 14, the anion was found to diffuse faster than the cation.

3.5   Overestimated Melting Points

As discussed earlier, the experimental melting points of $[C_2MIM][PF_6]$ and $[C_4MIM][PF_6]$ were accurately reproduced by the simulations. However, for $[C_nMIM][PF_6]$ with n=10, 12 and 14, although the trend was correctly captured, the calculated melting temperatures were found to be 80-90 K higher than the corresponding experimental values. Effort has been made to study this systematic overestimation and possible reasons are discussed.

3.5.1   VdW Correction in AIMD Simulation

As shown in early sections, besides the importance of electrostatic interactions in ionic liquid systems, vdW interactions also play essential roles especially for the ILs having a long alkyl chain. However, this effect is not considered when the atomic partial charges

were derived in the AIMD simulations. To study this effect, an empirical van der Waals correction of the Grimme type[63] is considered in the AIMD simulation and new charges were derived for each IL following the same procedure described previously.[52] The results are provided in the Electronic Supplementary Information and summarized in Table 1 and Figure 1. As shown in the table and the figure, for $[C_2MIM][PF_6]$ and $[C_4MIM][PF_6]$, the total charges as well as individual charge on each atom are almost the same and the effect of vdW correction is negligible. For ILs with longer alkyl chains, on the other hand, the magnitude of the total charges were found to be slightly smaller when the vdW correction was included, suggesting stronger vdW interactions in these ILs than in $[C_2MIM][PF_6]$ and $[C_4MIM][PF_6]$, consistent with the discussion in the earlier sections. Using the new charges, the T_m were calculated for each IL and the results are shown in Figure 3. For $[C_2MIM][PF_6]$ and $[C_4MIM][PF_6]$, the computed T_m increased slightly but still agree with experimental results well. For the ILs with longer alkyl chains, on the other hand, the calculated T_m using the new partial charges are slightly reduced, but the computed T_m are still higher than the experimental values by about 70 degrees. These results suggest that the vdW correction in the DFT calculation is not the main reason for the overestimated melting points.

3.5.2   Rotation of Torsion Angles

The pseudosupercritical path (PSCP) method was used for the melting point calculation in the current work. This method has been carefully validated previously and has been successfully applied to systems with varied complexity.[51,64–67] One key task in melting point calculations using either the PSCP method or other molecular simulation-based methods is to avoid the superheating caused mainly by the intermolecular interactions.[51] In the PSCP method, this is done by scaling down the electrostatic and van der Waals interactions in the crystal phase and generating a weakly interacting intermediate state along a reversible thermodynamic cycle. Phase change is controlled to take place in such weakly interacted condition so that the free energy barrier associated with superheating is minimized.[51] However, as shown earlier, in addition to nonbonded interactions, the bonded energy also makes a significant contribution to the fusion enthalpies in $[C_nMIM][PF_6]$ with n=10, 12 and 14. As shown in Table 3, the energy differences between the solid and liquid phases contributed

from the bonded energy is 20% or more of that of the nonbonded energies, which suggests that the bonded energy terms may also have contribution to the free energy barrier causing the superheating phenomenon. Further analysis found that the energy changes upon phase change due to dihedral angles contribute about half of ΔE_{bonded} with the other half from bond, angle and improper dihedral terms (data not shown). Considering the fact that the force constants for dihedral angles are generally one order of magnitude lower than those for angles and two orders of magnitude lower than those for bonds, the relative large energy change in dihedral angle terms upon melting of the crystals indicates significant torsional motion during the phase change.

Table 5 summarizes the dihedral angles associated with the alkyl chain in the cation molecules in the experimental crystal structure. The corresponding angles in each IL were found to be similar although the alkyl chain lengths differ significantly. The two dihedral angles involving imidazolium ring atoms, C5-N1-C7-C8 and N2-C7-C8-C9 (see Figure 2 for atomic labels), both have values around 60-70 degrees. Most of the dihedrals in the alkyl chain prefer anti-conformation ($\sim$ 180 degrees). The only exception is C8-C9-C10-C11, which takes gauche conformation ($\sim$ 60 degrees).

The dihedral angle distribution in the liquid phase was analyzed for each IL based on the simulated trajectories. The results are shown in Figure 7. Similar to the crystal phase, for each dihedral angle, the distributions were found to be similar in all ILs. Dihedral C5-N1-C7-C8 has a relatively even distribution with $\pm$ 60 degrees slightly preferred and zero degree prohibited. The other three dihedrals shown in the figure have similar distributions in which the anti-conformation is the dominant structure and the gauche conformation is the secondary. The relative weights of the two distributions vary slightly as shown by the integration curves. The distributions of all other dihedral angles in the alkyl chain were found to be similar to these three due to the similarity in the force field parameters.

Comparison of the values in the crystal phase and the distributions in the liquid phase clearly shows that most of the dihedral angles experience significant torsional motion upon melting. In the crystal phase, the dihedral angels formed by N1-C7-C8-C9 and C8-C9-C10-C11 are in a gauche conformation while all other dihedral angles are in an anti-conformation. Upon melting, all dihedral angles show a distribution between anti- and gauche. The free

energy barrier due to such conformational change can be a reason for the overestimated T_m.

The original PSCP method does not consider such free energy barriers explicitly. To study the effect of these torsional motions on the calculated melting points, the PSCP procedure was revised and the dihedral angle force constants were scaled to zero linearly in the first step (crystal to weakly interacted crystal) of the PSCP cycle[51] together with the scaling of the nonbonded interactions. The dihedral angles were later restored in the last step (weakly interacting liquid to liquid) of the cycle. The corresponding free energy change was calculated using the thermodynamic integration method in the same manner as used in the original PSCP method.[51] With this extra step in the PSCP method, the T_m of each IL was determined and the results are shown in Figure 3. As shown in the figure, the new results almost overlap with those without considering the effect of dihedral angles. This rules out the possibility that the overestimated melting points are caused by the free energy barrier due to the dihedral angle changes.

3.5.3 Finite Size Effect

It is known that long alkyl chains on cations lead to nanoscale ordering of non-polar domains in ILs.[28,29,31] It is also known experimentally that for very long alkyl chains, a liquid crystalline phase is observed.[48] It may be that in the actual system, long-range ordering of the chains occurs in a "pre-liquid crystalline" state, and the simulation box size used is too small to capture this effect. The system size effect was thus studied. Due to the increased cost of computational time on the bigger box, simulations were carried out only on $[C_4MIM][PF_6]$ and $[C_{10}MIM][PF_6]$. A simulation box containing 686 pairs of $[C_4MIM][PF_6]$ and 400 pairs of $[C_{10}MIM][PF_6]$ were used, respectively. Using the same PSCP method, the T_m were calculated to be 283 K for $[C_4MIM][PF_6]$ and 387 K $[C_{10}MIM][PF_6]$, respectively, almost the same as the results using the smaller simulation systems. It may be that even larger systems are needed to observe pre-ordering phenomenon but these are currently too computationally expensive to run.

In experiments, defects and impurities in a crystal can decrease the measured T_m significantly.[51] Such defects and impurities are usually at very low density. Due to the limited size of the simulation system even in these enlarged simulation boxes, such effect in experiments

14

can not be captured in the simulation, which can be another reason of the overestimated T_m.

It is worth mentioning that, in spite of the overestimated T_m for $[C_{10}MIM][PF_6]$, $[C_{12}MIM][PF_6]$ and $[C_{14}MIM][PF_6]$, the trend that the T_m increase as the alkyl chain becomes longer was correctly predicted.

4   Concluding Remarks

Using molecular dynamics simulation, the melting points of a series of imidazolium hexafluorophosphate based ionic liquids $[C_nMIM][PF_6]$ with n = 10, 12 and 14 were studied and the results were compared with earlier calculations in which T_m was accurately predicted for n=2 and n=4. The general Amber force field (GAFF) combined with atomic partial charges derived from ab initio molecular dynamics (AIMD) simulations on the crystal phases of each IL was used to describe the interactions in the system. This combination of force fields has been found to be reliable for similar systems.[52] Using the pseudosupercritical path (PSCP) method, the T_m of these ILs were calculated. It was found that the T_m of these ILs increase with increased alkyl chain length in the cation, consistent with the trend observed in experiments.[11,58] This trend is opposite to that of ILs with short alkyl chains such as $[C_2MIM][PF_6]$ and $[C_4MIM][PF_6]$. Between $[C_2MIM][PF_6]$ and $[C_4MIM][PF_6]$, the latter has a longer alkyl chain and lower T_m, which were also captured by the same PSCP method.[52]

The fusion enthalpies and fusion entropies were computed for each IL $[C_nMIM][PF_6]$ with n = 2, 4, 10, 12 and 14, respectively. It was found that the trends observed in the T_m are the result of a balance between fusion enthalpy and fusion entropy. For small ILs $[C_2MIM][PF_6]$ and $[C_4MIM][PF_6]$, the fusion enthalpies are similar and the fusion entropies governs the T_m trend. As a result, relative to $[C_2MIM][PF_6]$, $[C_4MIM][PF_6]$ despite having a higher fusion enthalpy, has a lower T_m. Whereas for ILs with a long alkyl chain $[C_nMIM][PF_6]$ with n = 10, 12 and 14, the fusion enthalpies increase more significantly than the fusion entropies as the alkyl chain becomes longer. As such, fusion enthalpies play the dominant role in deciding the melting temperature for these ILs, and the T_m increases

monotonically with chain length.

Cohesive energy analysis revealed that the increased fusion enthalpies in $[C_nMIM][PF_6]$ with n = 10, 12 and 14 are mainly due to enhanced van der Waals interactions, which is obviously caused by the hydrophobic carbon chains. At the same time, energy differences from bond, angle and dihedral angle terms between the solid and liquid phases, as a result of intramolecular conformation change during the phase change, also make significant contributions to the fusion enthalpies. This is different from the case in the enthalpy of vaporization. The increased enthalpy of vaporization of these ILs are almost completely governed by the van der Waals energy differences in the two phases and the role of bonded energy terms are negligible.

In spite of the correctly predicted trend in melting points, the calculated melting temperatures for $[C_nMIM][PF_6]$ with n = 10, 12 and 14 are systematically higher than the experimental values. Although it does not affect the conclusions discussed above, three possible reasons for the difference were investigated: 1) the effect of the vdW correction to the AIMD simulation used to derive the atomic partial charges; 2) the effect of the rotation of torsion angles upon melting of the crystal in the PSCP method; and 3) the effect of the finite size of the simulation system. Unfortunately, the computed T_m were found to be insensitive to all these factors. Another possible reason for the difference between simulation and experiment is related to the fact that there are always defects and/or impurities in crystals used in experiments although the density of such defects or impurities is usually extremely low. Due to the limited size of the simulation system, such effects was not studied in the current work. Further simulation or experimental work are needed to clarify the reason of the overestimated melting points in these systems. Future studies will also benefit from the recent progress in the density functional theory.[68]

Acknowledgment

puting (CRC) at the University of Notre Dame.

References

[1] P. Wasserscheid, *J. Ind. Eng. Chem.*, 2007, **13**, 325–338.

[2] N. Plechkova and K. R. Seddon, *Chem. Rev.*, 2008, **37**, 123–150.

[3] S. Zhang, X. Lu, Y. Zhang, Q. Zhou, J. Sun, L. Han, G. Yue, X. Liu, W. Cheng, and S. Li in *Molecular thermodynamics of complex systems*, ed. Lu, X and Hu, Y, Vol. 131 of *Structure and Bonding;* 2009; pp. 143–191.

[4] J. P. Hallett and T. Welton, *Chem. Rev.*, 2011, **111**, 3058–3576.

[5] K. Wendler, F. Dommert, Y. Zhao, R. Berger, C. Holm, and L. Delle Site, *Faraday Discuss.*, 2012, **154**, 111–132.

[6] H. Wang, G. Gurau, and R. D. Rogers, *Chem. Soc. Rev.*, 2012, **41**, 1519–1537.

[7] B. Bhargava, S. Balasubramanian, and M. L. Klein, *Chem. Comm.*, 2008, pp. 3339–3351.

[8] E. J. Maginn, *J. Phys.: Condens. Matter*, 2009, **21**(37), 373101.

[9] F. Dommert, K. Wendler, R. Berger, L. Delle Site, and C. Holm, *ChemPhysChem*, 2012, **13**, 1625–1637.

[10] P. Bonhôte, A.-P. Dias, N. Papageorgiou, K. Kalyanasundaram, and M. Gratzel, *Inorg. Chem.*, 1996, **35**, 1168–1178.

[11] W. M. Reichert, J. D. Holbrey, R. P. Swatloski, K. E. Gutowski, A. E. Visser, M. Nieuwenhuyzen, K. R. Seddon, and R. D. Rogers, *Crystal. Growth Design*, 2007, **7**, 1106–1114.

[12] P. A. Hunt, *J. Phys. Chem. B*, 2007, **111**, 4844–4853.

[13] S. Zahn, B. J. Thar, and B. Kirchner, *Phys. Chem. Chem. Phys.*, 2008, **10**, 6921–6924.

[14] K. Fumino, A. Wulf, and R. Ludwig, *Angew. Chem. Int. Ed.*, 2008, **47**(45), 8731–8734.

[15] E. I. Izgorodina, R. Maganti, V. Armel, P. M. Dean, J. M. Pringle, K. R. Seddon, and D. R. MacFarlane, *J. Phys. Chem. B*, 2011, **115**, 14688–14697.

[16] Y. Zhang and E. J. Maginn, *Phys. Chem. Chem. Phys.*, 2012, **14**, 12157–12164.

[17] J. D. Holbrey and K. R. Seddon, *J. Chem. Soc., Dalton Trans.*, 1999, **1999**, 2133–2139.

[18] J. G. Huddleston, A. E. Visser, W. M. Reichert, H. D. Willauer, G. A. Broker, and R. D. Rogers, *Green Chem.*, 2001, **3**, 156–164.

[19] A. E. Bradley, C. Hardacre, J. D. Holbrey, S. Johnston, S. E. J. McMath, and M. Nieuwenhuyzen, *Chem. Mater.*, 2002, **14**, 629–635.

[20] C. J. Margulis, *Mol. Phys.*, 2004, **102**, 829–838.

[21] H. Tokuda, K. Hayamizu, K. Ishii, M. A. B. H. Susan, and M. Watanabe, *J. Phys. Chem. B*, 2005, **109**, 6103–6110.

[22] K. Shimizu, M. Tariq, M. F. C. Gomes, L. P. N. Rebelo, and J. N. C. Lopes, *J. Phys. Chem. B*, 2010, **114**, 5831–5834.

[23] S. Tsuzuki, H. Matsumoto, W. Shinoda, and M. Mikami, *Phys. Chem. Chem. Phys.*, 2011, **13**, 5987–5993.

[24] A. Pensado, M. F. C. Gomes, J. N. Canongia Lopes, P. Malfreyt, and A. A. H. Padua, *Phys. Chem. Chem. Phys.*, 2011, **13**, 13518–13526.

[25] C. Ridings, V. Lockett, and G. Andersson, *Phys Chem Chem Phys*, 2011, **13**, 17177–17184.

[26] E. Binetti, A. Panniello, L. Triggiani, R. Tommasi, A. Agostiano, M. L. Curri, and M. Striccoli, *J. Phys. Chem. B*, 2012, **116**, 3512–3518.

[27] Y. Ji, R. Shi, Y. Wang, and G. Saielli, *J. Phys. Chem. B*, 2013, **117**, 1104–1109.

[28] S. M. Urahata and M. C. Ribeiro, *J. Chem. Phys.*, 2004, **120**, 1855–1863.

[29] Y. Wang and G. Voth, *J. Am. Chem. Soc.*, 2005, **127**(35), 12192–12193.

[30] J. N. A. C. Lopes and A. A. H. Padua, *J. Phys. Chem. B*, 2006, **110**, 3330–3335.

[31] A. Triolo, O. Russina, H.-J. Bleif, and E. Di Cola, *J. Phys. Chem. B*, 2007, **111**, 4641–4644.

[32] Z. Hu and C. J. Margulis, *Proc. Natl. Acad. Sci. U.S.A.*, 2007, **104**, 9546.

[33] A. Triolo, O. Russina, B. Razio, R. Triolo, and E. Di Cola, *Chem. Phys. Lett.*, 2008, **457**, 362–365.

[34] D. Xiao, L. G. Hines, S. Li, R. A. Bartsch, E. L. Quitevis, O. Russina, and A. Triolo, *J. Phys. Chem. B*, 2009, **113**, 6426–6433.

[35] K. Shimizu, M. F. Fosta Gomes, A. A. H. Padua, R. L. P. N., and J. N. C. Lopes, *J. Mol. Struct: THEOCHEM*, 2010, **946**, 70–76.

[36] M. Macchiagodena, F. Ramondo, A. Triolo, L. Gontrani, and R. Caminiti, *J. Phys. Chem. B*, 2012, **116**, 13448–13458.

[37] C. Hardacre, J. D. Holbrey, C. L. Mullan, T. G. Youngs, and D. T. Bowron, *J. Chem. Phys.*, 2010, **133**, 074510.

[38] H. V. R. Annapureddy, H. K. Kashyap, P. M. De Biase, and J. Margulis, Claudio, *J. Phys. Chem. B*, 2010, **114**, 16838–16846.

[39] O. Russina and A. Triolo, *Faraday Discuss.*, 2012, **154**, 97–109.

[40] R. Hagiwara and Y. Ito, *J. Fluorine Chem.*, 2000, **105**, 221–227.

[41] T. Umecky, M. Kanakubo, and Y. Ikushima, *J. Mol. Liquids*, 2005, **119**, 77–81.

[42] M. Tariq, P. J. Carvalho, J. A. P. Coutinho, I. M. Marrucho, J. N. C. Lopes, and P. N. Rebelo, Luis, *Fluid Phase Equilib.*, 2011, **301**, 22–32.

[43] L. M. N. B. F. Santos, J. N. C. Lopes, J. A. P. Coutinho, J. M. S. S. Esperanca, L. R. Gomes, I. M. Marrucho, and L. P. N. Rebelo, *J. Am. Chem. Soc.*, 2007, **129**, 284–285.

[44] T. Koddermann, D. Paschek, and R. Ludwig, *ChemPhysChem*, 2008, **9**, 549–555.

[45] D. H. Zaitsau, S. P. Verevkin, V. N. Emelyanenko, and A. Heintz, *ChemPhysChem*, 2011, **12**, 3609–3612.

[46] M. A. A. Rocha, C. F. R. A. C. Lima, L. R. Gomes, B. Schroder, J. A. P. Coutinho, I. M. Marrucho, J. M. S. S. Esperanca, L. P. N. Rebelo, K. Shimizu, J. N. C. Lopes, and L. M. N. B. F. Santos, *J. Phys. Chem. B*, 2011, **115**, 10919–10926.

[47] S. P. Verevkin, D. H. Zaitsau, V. N. Emel'yanenko, A. V. Yermalayeu, C. Schick, H. Liu, E. J. Maginn, S. Bulut, I. Krossing, and R. Kalb, *J. Phys. Chem. B*, 2013, **117**, 6473–6486.

[48] J. D. Holbrey and K. R. Seddon, *Clean Products and Processes*, 1999, **1**, 223–236.

[49] I. Krossing, J. M. Slattery, C. Daguenet, P. J. Dyson, A. Oleinikova, and H. Weingaertner, *J. Am. Chem. Soc.*, 2007, **129**(36), 11296.

[50] F. Gharagheizi, P. Ilani-Kashkouli, and A. H. Mohammadi, *Fluid Phase Equilib.*, 2012, **329**, 1–7.

[51] Y. Zhang and E. J. Maginn, *J. Chem. Phys.*, 2012, **136**, 144116.

[52] Y. Zhang and E. J. Maginn, *J. Phys. Chem. B*, 2012, **116**, 10036–10048.

[53] S. Plimpton, *J. Comp. Phys.*, 1995, **117**, 1–19.

[54] J. Wang, R. M. Wolf, J. W. Caldwell, P. A. Kollman, and D. A. Case, *J. Comput. Chem.*, 2004, **25**, 1157–1174.

[55] Z. Liu, S. Huang, and W. Wang, *J. Phys. Chem. B*, 2004, **108**, 12978–12989.

[56] U. C. Singh and P. A. Kollman, *J. Comput. Chem.*, 1984, **5**, 129–145.

[57] S. Dibrov and J. K. Kochi, *Acta Crystallo.*, 2006, **C62**, o19–o21.

[58] C. M. Gordon, J. D. Holbrey, A. R. Kennedy, and K. R. Seddon, *J. Mater. Chem.*, 1998, **8**, 2627–2636.

[59] CPMD, http://www.cpmd.org/, Copyright IBM Corp 1990-2008, Copyright MPI fur Festkorperforschung Stuttgart 1997-2001.

[60] W. G. Hoover, *Phys. Rev. A*, 1985, **31**, 1695–1697.

[61] W. Shinoda, M. Shiga, and M. Mikami, *Phys. Rev. B*, 2004, **69**, 134103.

[62] K. Dong, S. Zhang, D. Wang, and X. Yao, *J. Phys. Chem. A*, 2006, **110**, 9775–0782.

[63] S. Grimme, *J. Comput. Chem.*, 2006, **27**, 1787–1799.

[64] D. Eike, J. Brennecke, and E. Maginn, *J. Chem. Phys.*, 2005, **122**(1), 014115.

[65] D. Eike and E. Maginn, *J. Chem. Phys.*, 2006, **124**(16), 164503.

[66] S. Jayaraman and E. J. Maginn, *J. Chem. Phys.*, 2007, **127**(21), 214504.

[67] Y. Zhang and E. J. Maginn, *J. Chem. Theory Comput.*, 2013, **9**, 1592–1599.

[68] S. Grimme, W. Hujo, and B. Kirchner, *Phys. Chem. Chem. Phys.*, 2012, **14**, 4875–4883.

[69] U. Domanska and A. Marciniak, *J. Chem. Eng. Data*, 2003, **48**, 451–456.

[70] T. Umecky, M. Kanakubo, and Y. Ikushima, *Fluid Phase Equilib.*, 2005, **228-229**, 329–333.

Table 1: Calculated total charges (absolute values in e) on cations and anions based on AIMD calculations on crystal phases, without (AIMD) or with vdW (AIMD/vdW) correction.

IL	AIMD	AIMD/vdW
$[C_2MIM][PF_6]$	0.803	0.805
$[C_4MIM][PF_6]$	0.799	0.797
$[C_{10}MIM][PF_6]$	0.889	0.850
$[C_{12}MIM][PF_6]$	0.902	0.868
$[C_{14}MIM][PF_6]$	0.898	0.862

Table 2: Summary of the calculated fusion enthalpies (ΔH_f) and fusion entropies (ΔS_f) for the ionic liquids $[C_n MIM][PF_6]$ based on molecular dynamics simulations.

IL	ΔH_f (kJ/mol)		ΔS_f (J/mol/K)	
	Calc.	Exp.	Calc.	Exp.
$[C_2 MIM][PF_6]$	17.32±0.58	17.87[a]	52.51±1.76	52.84[b]
$[C_4 MIM][PF_6]$	17.95±0.69	19.87[c]	63.22±2.43	70.00[d]
$[C_{10} MIM][PF_6]$	39.16±1.10		99.91±2.81	
$[C_{12} MIM][PF_6]$	48.74±1.22	27.28[e]	118.62±2.97	81.92[f]
$[C_{14} MIM][PF_6]$	58.37±1.32	31.30[g]	133.26±3.01	89.41[h]

[a]Experimental value from Ref.[69]

[b]Experimental value from Ref.[69]

[c]Experimental value from Ref.[69]

[d]Experimental value from Ref.[69]

[e]Experimental value from Ref.[58]

[f]Experimental value from Ref.[58]

[g]Experimental value from Ref.[58]

[h]Experimental value from Ref.[58]

24

Table 3: The calculated energy differences between the solid and liquid phases (kJ/mol) at 298 K for the ionic liquids $[C_nMIM][PF6]$. The statistical errors are indicated in the parentheses for the last digits (i.e. $16.90(5) = 16.90 \pm 0.05$). E_{pot}, E_{bonded}, E_{nb}, E_{elec} and E_{vdW} represents potential energy, bonded energy, nonbonded energy, electrostatic energy and van der Waals energy, respectively.

IL	ΔE_{pot}	ΔE_{bonded}	ΔE_{nb}	ΔE_{elec}	ΔE_{vdW}
$[C_2MIM][PF_6]$	16.90(5)	0.38(4)	16.53(3)	9.50(2)	7.07(2)
$[C_4MIM][PF_6]$	17.57(8)	1.21(7)	16.36(4)	6.86(2)	9.50(3)
$[C_{10}MIM][PF_6]$	38.07(11)	6.32(10)	31.76(5)	13.51(3)	18.24(5)
$[C_{12}MIM][PF_6]$	53.30(12)	10.38(10)	42.93(6)	15.36(3)	27.57(5)
$[C_{14}MIM][PF_6]$	63.68(12)	13.47(11)	50.21(6)	17.03(3)	33.18(5)

Table 4: The calculated energy differences between the vapor and liquid phases (ΔH_{vap}, kJ/mol) at 298 K for the ionic liquids $[C_nMIM][PF_6]$. The statistical errors are provided explicitly or indicated in the parentheses for the last digits. (i.e. $141.75(7) = 141.75 \pm 0.07$). E_{pot}, E_{bonded}, E_{nb}, E_{elec} and E_{vdW} represents potential energy, bonded energy, nonbonded energy, electrostatic energy and van der Waals energy, respectively.

IL	ΔH_{vap}	ΔE_{pot}	ΔE_{bonded}	ΔE_{nb}	ΔE_{elec}	ΔE_{vdW}
$[C_2MIM][PF_6]$	140.59±0.75	141.75(7)	2.80(6)	138.95(3)	79.20(3)	59.75(2)
$[C_4MIM][PF_6]$	140.78±0.85	142.00(8)	-1.92(7)	143.93(3)	74.56(3)	69.33(2)
$[C_{10}MIM][PF_6]$	189.23±1.05	186.82(10)	-0.08(9)	186.86(4)	86.15(3)	100.75(3)
$[C_{12}MIM][PF_6]$	201.63±1.11	202.92(10)	4.48(10)	198.45(4)	86.48(3)	111.96(3)
$[C_{14}MIM][PF_6]$	212.17±1.16	206.10(11)	-1.42(10)	207.48(4)	84.39(3)	123.14(3)

Table 5: Dihedral angle values (degree) in the experimental crystal structures of ionic liquids $[C_nMIM][PF_6]$.

n	2	4	10	12	14
C5-N1-C7-C8	61.30	71.17	65.07	66.41	66.55
N1-C7-C8-C9		60.81	66.41	66.70	66.28
C7-C8-C9-C10		178.06	176.56	176.31	175.98
C8-C9-C10-C11			59.85	60.15	60.79
C9-C10-C11-C12			173.61	172.54	173.00
C10-C11-C12-C13			176.66	177.34	177.20
C11-C12-C13-C14			179.21	179.73	179.27
C12-C13-C14-C15			176.82	177.27	177.84
C13-C14-C15-C16			179.76	178.79	179.51
C14-C15-C16-C17				177.91	178.78
C15-C16-C17-C18				179.88	179.64
C16-C17-C18-C19					178.68
C17-C18-C19-C20					179.05

Figure captions

Figure 1 The derived partial charges for $[C_nMIM][PF_6]$ using the AIMD method without (top left) and with (top right) vdW correction, respectively. The lower panels show the partial charges of the P (left) and F (right) atoms as function of alkyl chain length in the cation. Lines are added to guide the eye.

Figure 2 The labeling of heavy atoms in $[C_{14}MIM][PF_6]$. The labeling is similar in other ILs.

Figure 3 The computed melting points for ionic liquids $[C_nMIM][PF_6]$ using the PSCP procedure. Partial charges derived from AIMD simulation on the crystal phases, without (AMID) or with vdW (AIMD/vdW) correction, were used in the simulations. The results calculated using a revised PSCP procedure (AIMD/dihe) are also shown in which the dihedral angle force constants were scaled to zero in the first step and restored in the last step of the PSCP cycle. Experimental melting points are provided for comparison.

Figure 4 The calculated spatial distribution of anion center of mass around cation in $[C_2MIM][PF_6]$ and $[C_4MIM][PF_6]$.

Figure 5 The computed radial distribution functions (RDFs) at 500K for $[C_nMIM][PF_6]$ ILs. Left column: center of mass RDFs. Right column: site-specific RDFs. Note that CT is the terminal carbon on the longest alkyl chain of the cation.

Figure 6 The computed self-diffusion coefficients for ionic liquids $[C_nMIM][PF_6]$ (filled symbols for the cations and open symbols for the anions). Dynamics becomes slower when the alkyl chain in the cation becomes longer. Available experimental results[70] (black) are included for comparison.

Figure 7 The computed dihedral angle distribution in liquid $[C_nMIM][PF_6]$ at 500 K using the partial charges derived from AIMD simulation on the crystal structures. Integration of each distribution was shown as dashed line (right axis).
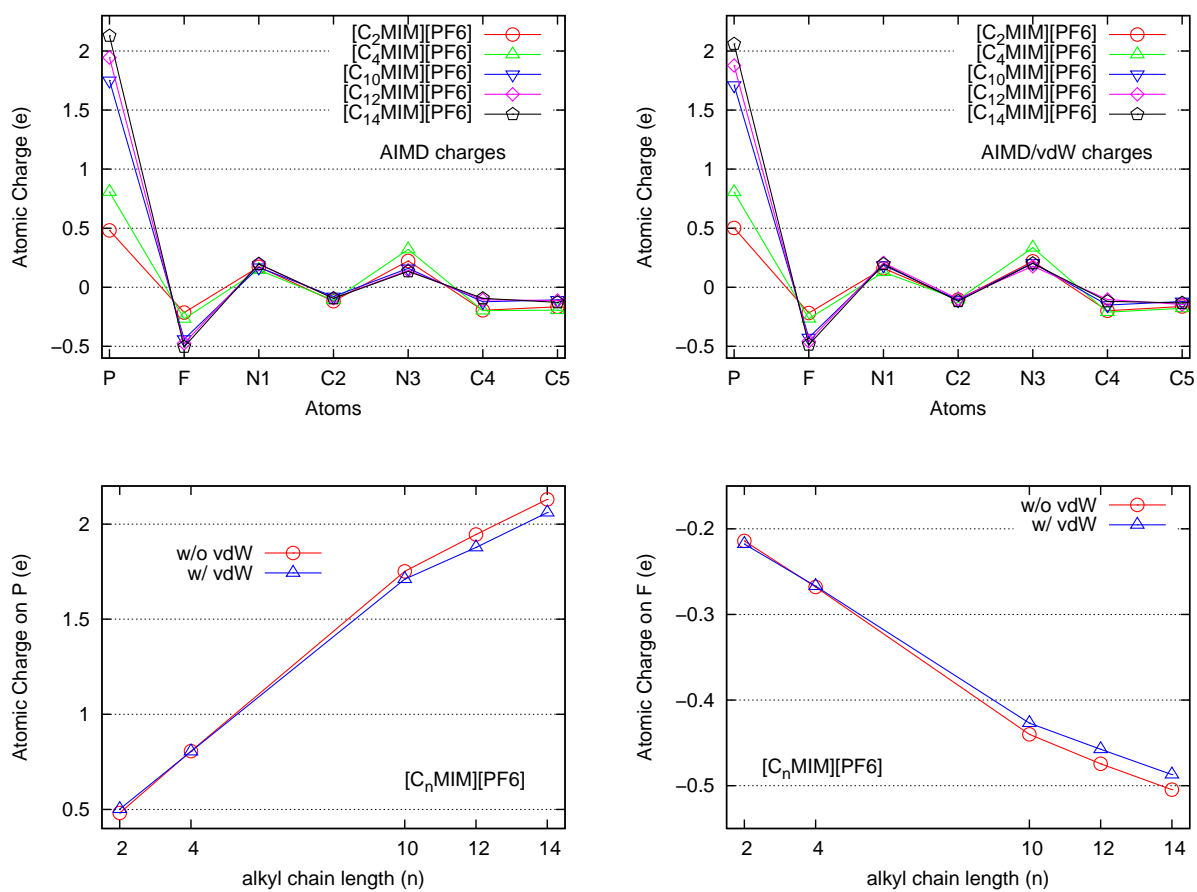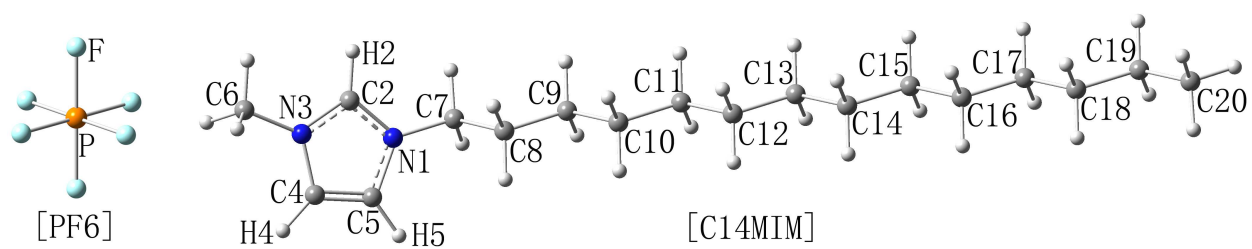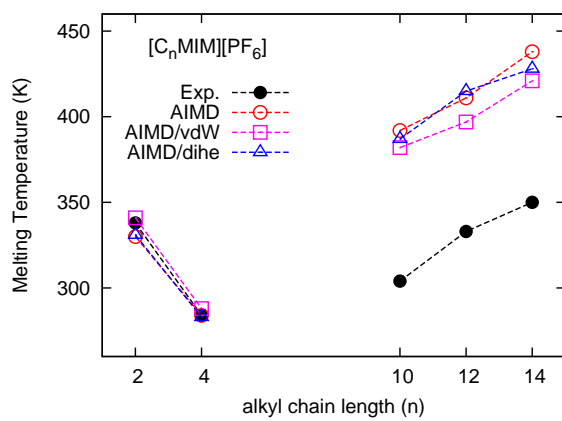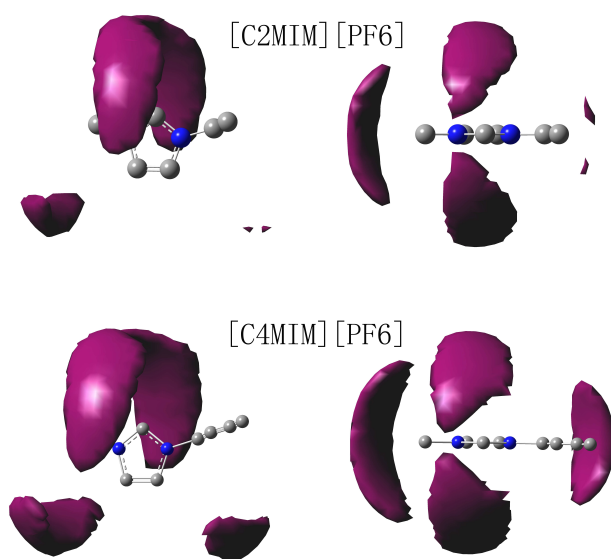
Figure 1:

Figure 2:

Figure 3:
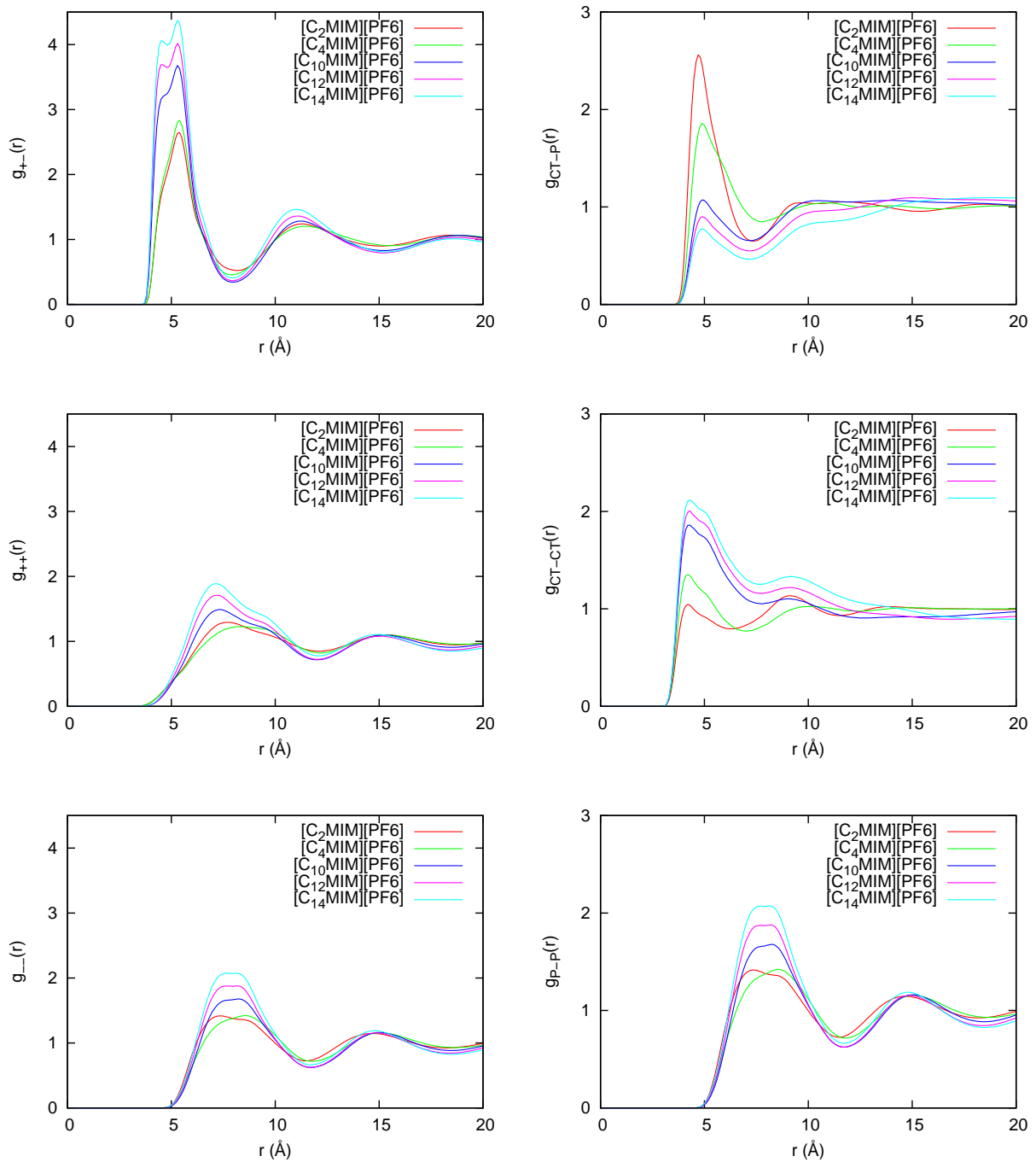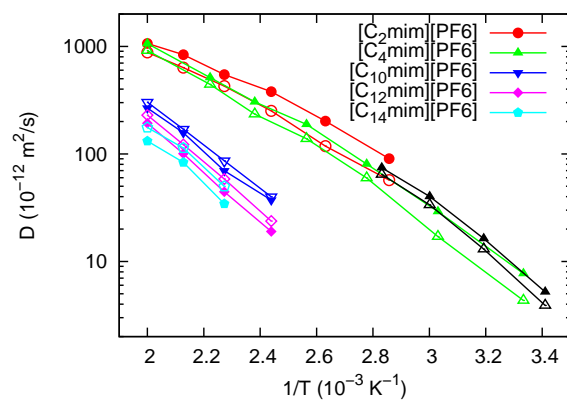
[C2MIM][PF6]

[C4MIM][PF6]
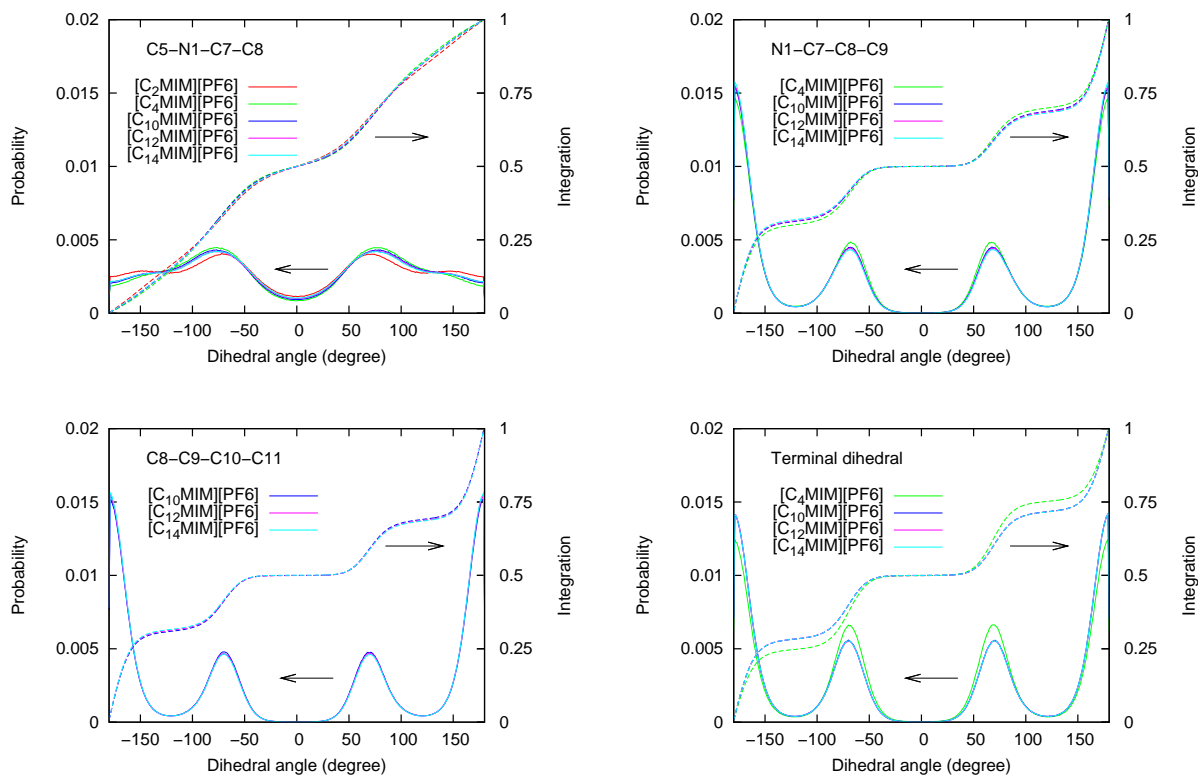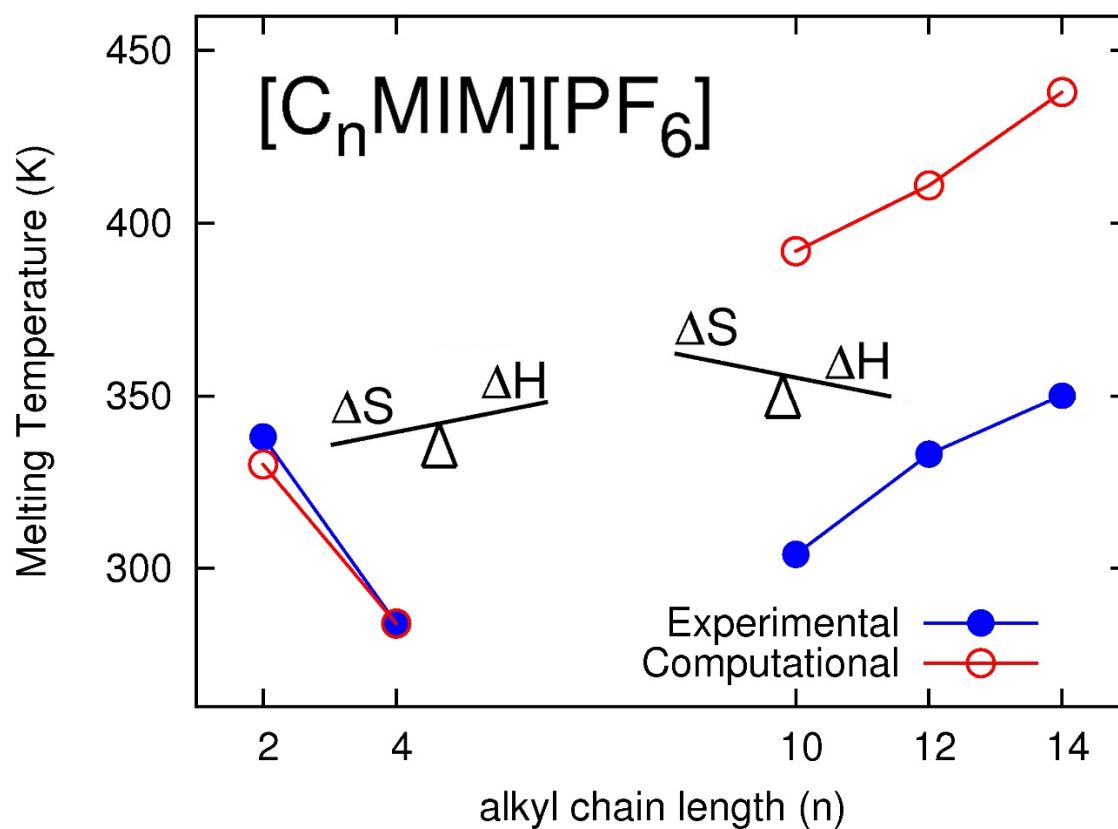
Figure 4:

Figure 5:

Figure 6:

Figure 7:

Experimental trends in melting points correctly captured by simulation and the opposite trends were found to be the results of the balance between fusion enthalpy and fusion entropy.